

**Magnetic fluctuation driven large enhancement of the thermopower
at a critical doping in magnetic semimetal $\text{Cr}_{1+\delta}\text{Te}_2$**

*Atwa Mohamed¹, Yuita Fujisawa¹, Takatsugu Onishi¹, Markel Pardo-Almanza¹, Mathieu Couillard¹,
Keita Harada¹, Tsunehiro Takeuchi², Yoshinori Okada¹*

¹Quantum Materials Science Unit, Okinawa Institute of Science and Technology (OIST),

Okinawa 904-0495, Japan

²Research Center for Smart Energy Technology, Toyota Technological Institute,

Nagoya 468-8511, Japan;

Abstract

$\text{Cr}_{1+\delta}\text{Te}_2$ is a self-intercalated transition metal dichalcogenide that hosts tunable electronic filling and magnetism in its semimetallic band structure. Recent angle-resolved photoemission spectroscopy (ARPES) studies have unveiled a systematic shift in this semimetallic band structure relative to the chemical potential with increased Cr doping. This report presents the temperature and magnetic field dependence of the longitudinal thermopower S_{xx} for different $\text{Cr}_{1+\delta}\text{Te}_2$ compositions. We show that as doping increases, the sign of S_{xx} changes from positive to negative at the critical doping level of $\delta \sim 0.5$. This observed doping-dependent trend in the thermopower is consistent with the evolution of the semimetallic band structure from ARPES. Importantly, an anomalous enhancement of the thermoelectric response is also observed around $\delta \sim 0.5$. Combining information from magnetometry and ARPES measurements, existence of the critical nature of the doping level δ_c (~ 0.5) is unveiled in magnetic semimetal $\text{Cr}_{1+\delta}\text{Te}_2$, where near-Fermi-energy pseudogap formation and magnetic fluctuations play a vital role in enhancing thermoelectric energy conversion.

Introduction

The thermoelectric effect enables the conversion of thermal energy to electricity¹. Asymmetry in the energy-dependent electronic conductivity between the hot and cold sides of a metallic conductor generates a driving force for a net flow of charge entropy. Whatever the microscopic origins of this entropy are, if they are coupled to charge carriers through inelastic scattering, one can imagine various intriguing ways to modulate thermoelectric effects. One well-known example is the phonon drag effect, in which the coupling between electrons and phonons can result in enhanced thermoelectricity. Manipulation of the magnetic degree of freedom is another attractive route to controlling the thermoelectric effect. For example, while a consensus has yet to be reached, a large spin entropy and anomalous electronic states near E_F have been proposed to explain the giant Seebeck effect of cobalt oxides^{2,3,4,5}. Efforts to simultaneously engineer the heat, spin, and charge degrees of freedom have resulted in the field of spin caloritronics, where spin currents control and enhance thermoelectric phenomena^{6, 7, 8, 9}. Magnetism-mediated enhancement of the thermoelectric response has also prompted investigations into the fundamental nature of thermoelectricity in ferromagnetic versus antiferromagnetic materials¹⁰. Research on the interaction between improved thermoelectric response and Berry curvature physics is also ongoing^{11,12,13}. Although these recent explorations of the exotic interplay between magnetism and the thermoelectric response are promising, a microscopic understanding of the coupling between magnetism and thermoelectricity is still in its infancy. To promote understanding of the interaction between spins and charges in thermoelectric materials, ideal materials to focus on are those with widely tunable electronic band filling and deeply controllable magnetic structure.

Transition-metal dichalcogenides (TMDs) are a unique platform for tuning electronic and magnetic properties in the 2D limit. The atomic layers of TMDs are weakly coupled through the van der Waals (vdW) force, creating an opportunity to chemically tune their physical properties by intercalating native atoms into the vdW gaps¹⁴. Among the magnetic TMDs, $\text{Cr}_{1+\delta}\text{Te}_2$ (**Fig. 1a**) is a promising self-intercalated ferromagnet with widely-tunable electronic and magnetic properties^{15,16,17,18,19,20,21,22,23,24,25,26,27,28,29,30,31,32,33}. Our recent efforts have yielded a unique recipe for the growth of epitaxial thin films of $\text{Cr}_{1+\delta}\text{Te}_2$ over a wide compositional range³⁴. Based on the previously reported phase diagram of this system, a Curie temperature (T_c) beyond room temperature is achieved as the intercalated Cr (δ) increases (**Fig. 1b left axis**). Furthermore, the effective magnetic anisotropy energy (K_{eff}), defined as the difference in energy to align spins along the in-plane (K_{in}) or out-of-plane (K_{out}) directions, shows a gradual change from positive to negative values as δ increases (**Fig. 1b right axis**). Density functional theory (DFT) calculations have suggested an inherent magnetic frustration from competing magnetic interactions, which plays a role in modulating K_{eff} in this system. In particular, significant magnetic fluctuations are expected at $K_{eff}\sim 0$ (**Fig. 1b**).

Recently, the doping-dependent electronic structure of $\text{Cr}_{1+\delta}\text{Te}_2$ has also been reported. Using in-situ angle-resolved photoemission spectroscopy (ARPES), a systematic energy shift of the semimetallic band portion was directly revealed around the zone boundary relative to the chemical potential (**Figs. 1c and d**)³⁵. ARPES measurements at 14 K (well below T_c) have yielded a characteristic energy (E_0) for the semimetallic band portion around the \bar{M} point (**Fig. 1d**). The Fermi energy E_F was shown to approach E_0 near a critical doping $\delta_c \sim 0.5$.

Alongside a metallic hole band near the $\bar{\Gamma}$ point at all doping levels, the formation of a pseudogap in the density of states (DOS) was predicted to occur around this critical composition. These ARPES findings prompted our current investigation of the doping-dependent longitudinal thermopower (S_{xx}), as its sign and absolute value should be sensitive probes of the existence of the pseudogap and its energy relative to the chemical potential. Another worthwhile motivation for measuring S_{xx} is to pursue any magnetism-driven enhancements to the thermopower that $\text{Cr}_{1+\delta}\text{Te}_2$ can be expected to host, being both magnetically and electronically tunable. However, the doping evolution of the thermoelectric response in the absence and presence of magnetic fields has not been investigated in $\text{Cr}_{1+\delta}\text{Te}_2$.

We report on the systematic measurement of S_{xx} and longitudinal electrical resistivity (ρ_{xx}) in magnetic semimetal $\text{Cr}_{1+\delta}\text{Te}_2$. We discuss the doping, temperature, and magnetic field evolution of S_{xx} with respect to the underlying band structure and magnetism. As the most significant finding in this study, we show that at the critical doping level of $\delta_c \sim 0.5$, a possible interaction between magnetic fluctuations and the formation of an anomalous electronic state at the chemical potential cooperatively leads to an enhancement of the thermoelectric properties in $\text{Cr}_{1+\delta}\text{Te}_2$.

Methods

Sample Preparation

The (001) oriented epitaxial $\text{Cr}_{1+\delta}\text{Te}_2$ films used in this work were grown on Al_2O_3 (0001) substrates with a molecular beam epitaxy (MBE) system through a two-step process that involved film deposition followed by post-deposition annealing in situ as described in our previous work. Following the same detailed characterization methods performed previously, the fraction of intercalated Cr(δ) was determined by combining energy-dispersive X-ray spectroscopy (EDS) of the elemental ratios and X-ray diffraction (XRD) estimates of the lattice constants. The thickness of all samples grown in this study was approximately 80 nm.

Transport Measurements

S_{xx} and ρ_{xx} were measured simultaneously using a Quantum Design PPMS® DynaCool system combined with a custom-built sample stage and electronics set-up. The electrode configuration is shown in **Fig. 2a**. In this study, technical limitations of the PPMS system and the samples restrict our S_{xx} measurements between 80 and 380 K. The lower temperature limit represents a threshold below which the Al_2O_3 substrate becomes too thermally conductive to maintain a sufficient temperature gradient and determine S_{xx} across the sample accurately. The vertical dotted lines in **Fig. 1b** indicate the doping levels studied in this report on the previously reported phase diagram. In this report, all magnetic fields were applied along the out-of-plane direction, as shown schematically in **Fig. 2a**.

Results and Discussion

Doping and temperature dependence of ρ_{xx} and S_{xx} in $B=0$

The temperature and doping dependence of ρ_{xx} and S_{xx} are shown in **Figs. 2b** and **c**, respectively. Regardless of the detailed microscopic origins, suppression of electron-spin scattering can be expected to occur in

magnetically-ordered states compared to paramagnetic states. Therefore, T_c at each doping level is estimated from the position of the kink in the $\rho_{xx}(T)$ curves, as indicated by the arrows in **Figs. 2b** and **c**. The estimated T_c values are consistent with those determined previously. The doping dependence of $S_{xx}(T)$ also exhibits several characteristic behaviors. The samples with $\delta=0.34$ and $\delta=0.4$ show positive values with a nearly linear T dependence (left two panels in **Fig. 2c**). In contrast, S_{xx} for $\delta=0.50$ and $\delta=0.54$ (middle panel in **Fig. 2c**) show negative values with a kink around T_c . Notably, such a kink structure around T_c is nearly absent in the highest doped sample, $\delta=0.68$ (right panel in **Fig. 2c**). Hereafter, we focus on S_{xx} , as the essential trends in $\rho_{xx}(T)$ are qualitatively similar for all doping levels. In the following sections, we elaborate on the doping-dependent sign change in $S_{xx}(T)$, followed by a discussion of the electronic and magnetic origins of the kink around T_c in the $S_{xx}(T)$ curves.

Mott formula for S_{xx}

The simplest model for the temperature dependence of thermopower S_{xx} in metals is the so-called Mott relation.

$$S_{xx} = \frac{\pi^2 k_B^2 T}{3e} \times \left\{ \frac{d \ln \sigma_{xx}(E)}{dE} \right\}_{E=E_F} = \frac{\pi^2 k_B^2 T}{3e} \left[\frac{1}{N(E_F)} \left\{ -\frac{dN(E)}{dE} \right\}_{E=E_F} + \frac{1}{\tau(E_F)} \left\{ \frac{d\tau(E)}{dE} \right\}_{E=E_F} \right] \quad (1)$$

Here, the spectral conductivity σ_{xx} is proportional to the density of states $N(E)$ and the scattering rate $\tau(E)$, based on the relaxation time approximation from Boltzmann transport theory. By assuming an energy-independent scattering rate τ in Equation (1), S_{xx} can be expressed as:

$$S_{xx} \approx \frac{\pi^2 k_B^2 T}{3e} \left[\frac{1}{N(E_F)} \left\{ -\frac{dN(E)}{dE} \right\}_{E=E_F} \right] \quad (2)$$

The above relation makes it evident that the sign of S_{xx} corresponds to that of $-dN(E)/dE_{E=E_F}$. In this case, if the chemical potential exists in a hole-like band ($-dN/dE > 0$ at E_F), the sign and slope of $S_{xx}(T)$ become correspondingly positive, while if the chemical potential exists in an electron-like band ($-dN/dE < 0$ at E_F), the sign and slope of $S_{xx}(T)$ become negative.

Relation between $S_{xx}(\delta)$ and band structure

To uncover the connection between the sign of S_{xx} and the corresponding band structure at each $\text{Cr}(\delta)$, we plot the doping dependence of S_{xx} at 350 K and its correlation with the doping evolution of the semimetallic band portion at the \bar{M} point (**Fig. 2d**). For a fair comparison, 350K is chosen to be above T_c for all doping levels. A sign change in S_{xx} at 350 K is evident as δ increases. Considering the semimetallic band around the \bar{M} point (**Fig. 1d**), $E_F(\delta)-E_0 > 0$ leads to $-dN/dE > 0$ and consequently to a positive sign in S_{xx} . On the other hand, $E_F(\delta)-E_0 < 0$ leads to $-dN/dE < 0$, corresponding to a negative sign in S_{xx} . Admittedly, this is a simplified picture that ignores the existence of bands other than the semimetallic band around the \bar{M} point. Moreover, this simplified picture deliberately excludes the nuance of a k_z dispersion relying solely on the band dispersion around the \bar{M} point probed using the single-photon energy available in our ARPES. Nevertheless, a correlation can clearly be seen between the sign of $E_F(\delta)-E_0$ and $S_{xx}(\delta)$. This correlation implies that the previously observed ARPES band

around the \bar{M} point in **Fig. 1c** governs the doping-dependent behavior of the thermoelectric properties in this system. Note that the doping dependence of normal Hall coefficient does not show sign change with doping δ in a previous report³⁴. However, this is not contradictory. While the normal Hall effect is more sensitive to electronic state anisotropy in momentum space at E_F ³⁶, S_{xx} is sensitive to electronic state anisotropy along energy axis relative to E_F .

Anomaly in S_{xx} around T_C

Next, we discuss the origin of the kink in the $S_{xx}(T)$ curves across T_C . Based on Equation (1), S_{xx} can be modulated by changes to both $N(E)$ and $\tau(E)$ by the magnetic phase transition. Before discussing these quantities, we first elaborate on the nature of magnetic fluctuations above T_C . Focusing on the magnetic field dependence of S_{xx} is a rational method of investigating the influence that magnetic fluctuations have on the thermoelectric response³⁷. **Fig. 3a** shows the S_{xx} under external field $B=0$ (filled symbol) and 9 T (empty symbol). For simplicity, data for only three doping levels $\delta=0.34, 0.50$ and 0.68 are shown in **Fig. 3a**. To quantify the magnetic field-dependent contribution, $|\Delta S_B(T)|=|S_{xx}(T)_{B=9T} - S_{xx}(T)_{B=0T}|$ is defined (see hatched area in **Fig. 3a**). The quantity $|\Delta S_B|$ can be considered as a measure of the magnetic fluctuation-related contributions to S_{xx} since the application of a magnetic field can be naturally suppresses magnetic fluctuations. Similar to the method shown in **Fig. 3a**, $|\Delta S_B(T)|$ for five doping levels are shown in **Fig. 3b**. From **Fig. 3b**, negligible magnetic field dependence is observed in the samples with $\delta=0.34$ and $\delta=0.4$. On the other hand, a prominent signal is observed at T_C in $|\Delta S_B|$ in the $\delta=0.5, 0.54,$ and 0.68 samples. Notably, the $|\Delta S_B|$ value at T_C are relatively similar between $\delta=0.5$ and 0.54 , whereas their values are clearly larger than $|\Delta S_B|$ at T_C in the $\delta=0.68$ sample. This observation indicates that S_{xx} responds more sensitively to an external magnetic field around $\delta=0.5$, which results in a maximum $|\Delta S_B|$ at T_C around this doping level.

Magnetic fluctuation driven enhancement of S_{xx}

Based on Equation (2), with T-independent density of states $N(E)$ near E_F , $S_{xx}(T)$ is reasonably described by T-linear behavior, unless unconventional magnetism related contribution is not involved. Thus for comparison with $|\Delta S_B|$, we phenomenologically quantify the change in S_{xx} across T_C by subtracting the extrapolated linear component from low-temperature behavior and define $|\Delta S_0|=|S_{xx} - S_{linear}|$ (see **Fig. 2c**). **Fig. 3c** shows a comparison between $|\Delta S_0|$ and $|\Delta S_B|$ at T_C . Note that $|\Delta S_B|$ is an extracted degree of magnetic fluctuation with changing magnetic field whereas $|\Delta S_0|$ is an extracted zero field enhanced quantity. If these two values agree well, magnetic fluctuation driven enhancement of zero field S_{xx} is expected to be supported. Indeed, as in **Fig. 3c**, a clear agreement is observed in the doping-dependent trends between $|\Delta S_0|$ and $|\Delta S_B|$ at T_C . Based on this agreement, therefore, we conclude that the origin of $|\Delta S_0|$ must also pertain to the nature of the magnetic fluctuations in $\text{Cr}_{1+\delta}\text{Te}_2$. Particular important fact is that such magnetic fluctuation-driven enhancement of S_{xx} becomes maximum around $\delta \sim 0.5$. Hereafter, we discuss the microscopic picture of the intertwined magnetic fluctuations and the enhancement in S_{xx} , focusing on the critical doping level $\delta \sim 0.5$, which we designate as δ_c .

Magnon vs. Spin Fluctuations around T_C

We begin by discussing the microscopic picture of the fluctuating magnetism around T_c . The conventional mean-field picture for explaining magnetism in metals is known as the Stoner model. In this model, spin-degenerate bands are split into majority and minority spin bands separated by an exchange energy that is associated with the energetic cost of transitioning from paramagnetic states ($T > T_c$) to magnetically ordered states ($T < T_c$)³⁸. An abrupt change in the band structure occurs near T_c per this interpretation. However, this conventional Stoner model can be excluded as the origin of the magnetic behavior in our system, as we observe signature of spin fluctuation far above T_c . As an alternative, we invoke the two pictures of the microscopic origins of magnetic fluctuations. In the first picture, the collective propagations of magnetic spin precessions, known as ‘magnons,’ emerge in localized magnetically ordered states. Although magnon excitations have been shown to persist above T_c in the so-called ‘paramagnon’ regime³⁹, the conventional formalism of magnons supports their dominant existence only below the Curie and Néel temperatures (T_c and T_N) of localized magnetically ordered systems⁴⁰. The second picture relies on spin fluctuation theory, which has succeeded in explaining the physical properties of itinerant magnetism in various materials⁴¹. Spin fluctuations in itinerant electron systems predominantly influence the thermodynamic properties of weakly or nearly ferromagnetic metals. Such spin fluctuations can survive well above T_c . Given that $|\Delta S_0|$ persists far above T_c (see **Fig. 4a**), we suspect that spin fluctuations in an itinerant magnetic system are the origin of $|\Delta S_0|$ around δ_c .

Indeed, the spin fluctuation picture is better supported by the temperature dependence of $|\Delta S_0|$ around T_c (**Fitting in Fig. 4a**). Our data indicate a logarithmic temperature dependence T^n with n greater than 5 for samples with $\delta > \delta_c$ (**Fig. 4b**). This exponent far exceeds the value predicted by a conventional magnon excitation scenario, which predicts an exponent of $n \sim 1.5$ for FMs and $n \sim 3$ for AFMs based on a quadratic magnon dispersion⁴². This interpretation of the origins of the magnetic enhancement in $|\Delta S_0|$ is consistent with previous studies on the Cr-Te system, where specific heat and magnetometry measurements of bulk samples support spin fluctuations rather than magnons as the better descriptor of magnetism in the Cr-Te system^{23, 43, 44, 45}. While fully differentiating between these two pictures is non-trivial in real-world magnetic materials, which exhibit aspects of both magnons and spin fluctuations, we lean more towards spin fluctuations in an itinerant magnetic picture as the description of magnetism in our samples near and above δ_c .

Nature of critical doping

Our most intriguing finding beyond the existing literature on the Cr-Te system is the existence of a critical doping (δ_c). From a previous DFT study, two distinct magnetic Cr sublattices are expected to coexist in samples with $\delta = 1$ (i.e., CrTe), each exhibiting its own long-range magnetic order. FM interactions couple Cr atoms along the in-plane direction on one sublattice, while AFM interactions couple Cr atoms along the out-of-plane direction on the other sublattice, as shown in **Fig. 4c**. Even in the absence of distinct sublattices, as in CrTe₂, recent calculations predict a competition between multiple magnetic interactions that influence the magnetic ground states and K_{eff} , a coupling that is quite sensitive to the lattice spacing⁴⁶. Therefore, the experimental realization of $K_{eff} \sim 0$ around δ_c is expected to reflect a particularly unique situation where the competition between multiple magnetic interactions and a correspondingly large frustration leads to enhanced magnetic fluctuations. In this situation, based on an itinerant magnetic picture, we can expect significant fluctuations of

spin density ρ_s in both space and time to survive far above T_C (**Fig. 4d**). Since it is well accepted that near- E_F electrons are coupled to and scattered by spin fluctuations in itinerant magnetic systems, it is natural to speculate that the enhanced magnetic fluctuations and their resultant entropy can drag electrons through inelastic scattering, analogous to the drag effects caused by phonons and magnons.

Electronic structure perspectives

We speculate that the spin fluctuation driven enhancement of S_{xx} around δ_c is also linked to the anomaly in the electronic state around this critical doping level. This notion is supported by the fact that $E_0-E_F=0$ is realized around $\delta_c \sim 0.5$. As indicated previously, while a metallic hole band occurs near the $\bar{\Gamma}$ point at all doping levels, a pseudogap in the density of states at E_F occurs exclusively at δ_c (see **Fig. 1c** and **d**). Therefore, we suspect that enhanced magnetic fluctuations alongside the pseudogap formation at E_F in the δ_c sample cooperatively drive the observed enhancement in the zero-field thermoelectric energy conversion around T_C . There are two paradigms by which to interpret such a cooperation. The first relies solely on the experimentally observed band structure around the \bar{M} point from ARPES, disregarding the energy dependence of the scattering rate $\tau(E)$. This picture is justified by the factor $1/N(E)$ in an application of Equation (2) to our observations, since the position $E_0-E_F = 0$ is expected to lead a dip in $N(E)$ (i.e., a pseudogap). A second and more holistic paradigm would be to consider the asymmetry in $\tau(E)$ relative to E_F , in addition to expected pseudogap in $N(E)$. For instance, such asymmetric $\tau(E)$ can be realized if a characteristic energy for an electronic state sensitive to the spin orientation and its fluctuations exists away from E_F . Although modeling of the microscopic underpinnings of these observations in S_{xx} is anticipated as a future undertaking, it can be expected that a significant spin-orbit coupling effect arising from the presence of the heavy element Te plays a dominant role in bridging between the spin and charge degrees of freedom near E_F in $\text{Cr}_{1+\delta}\text{Te}_2$.

Summary

A systematic investigation of the doping, temperature, and magnetic field dependence of the longitudinal thermoelectric response S_{xx} is presented in the electronically/magnetically tunable semimetal $\text{Cr}_{1+\delta}\text{Te}_2$. We show signatures of magnetic fluctuation-driven enhancement of longitudinal thermoelectric response S_{xx} around a critical doping level $\delta_c \sim 0.5$, where pseudogap formation and competition between coexistent magnetic interactions are expected to become dominant.

We emphasize that detection of a magnetically modulated thermoelectric signal necessitates coupling between the magnetic and charge degrees of freedom. While a solid understanding of the underlying electronic states is always crucial in interpreting such charge-spin coupling, direct spectroscopic evidence of the electronic structure has been lacking from most studies in magnetic/metallic thermoelectric materials so far. As such, this study, which bridges between momentum space electronic states and thermoelectric effects in the tunable magnetic semimetal $\text{Cr}_{1+\delta}\text{Te}_2$, provides valuable clarifying information regarding the interplay between magnetism and thermoelectricity. While the doping level around $\delta_c (\sim 0.5)$ has been the primary focus of this study, the possibility of systematic control between $\delta \sim 0$ (CrTe_2) and $\delta \sim 1$ (CrTe) is a unique characteristic of the $\text{Cr}_{1+\delta}\text{Te}_2$ system. Consequently, this study also showcases the merits of self-intercalated $\text{Cr}_{1+\delta}\text{Te}_2$ for

investigations of magnetically-enhanced thermoelectricity. The fact that $\text{Cr}_{1+\delta}\text{Te}_2$ has been identified as an intriguing material platform that hosts Berry curvature physics in real and momentum spaces also suggests the possibility of exotic intertwined effects between the anomalous thermoelectric response and Berry curvature physics to be pursued in future investigations of this material.

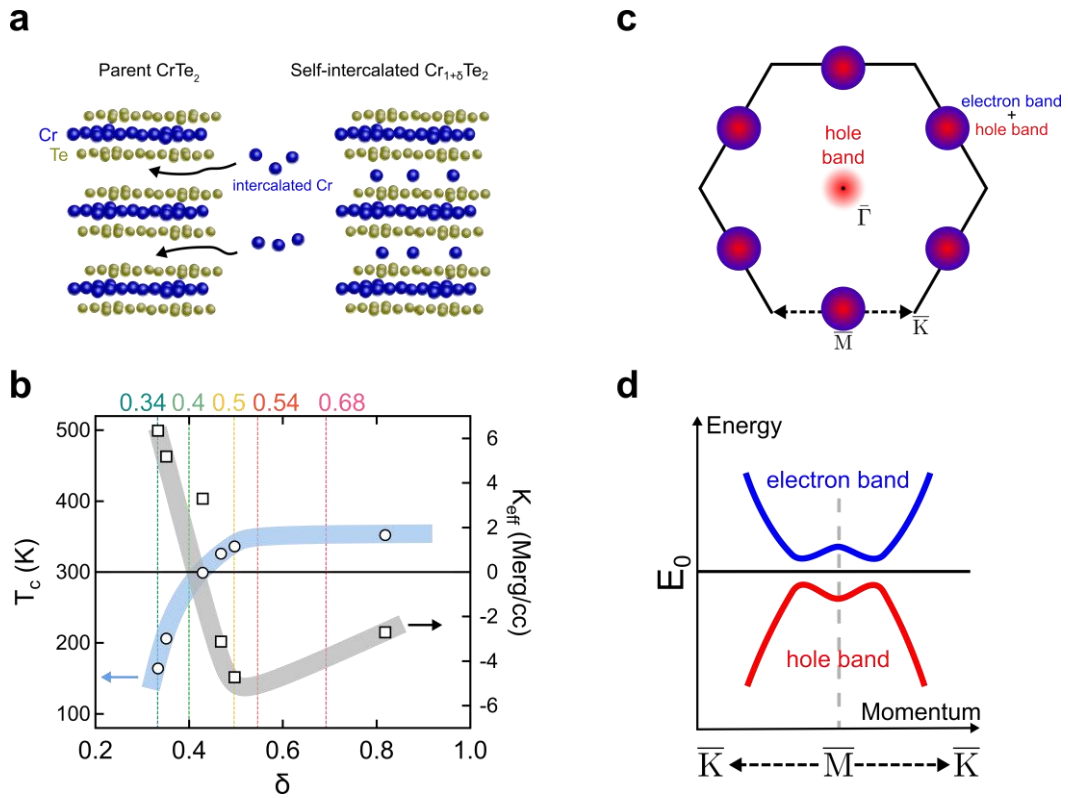


Fig. 1 Magnetic and electronic tunability of $\text{Cr}_{1+\delta}\text{Te}_2$. **a** Schematic for self-intercalation of Cr atoms in the parent CrTe_2 . **b** Doping evolution of the Curie temperature (T_c) and magnetic anisotropy energy (K_{eff}) as previously determined from³⁴. The colored lines indicate the compositions investigated in this study. **c** Schematic of the k -space electronic structure determined from ARPES studies on $\text{Cr}_{1+\delta}\text{Te}_2$ ³⁵. Around $\bar{\Gamma}$, the hole band dominates near the Fermi energy. However, the coexistence of electron and hole bands around \bar{M} points constitute a semimetallic band portion. **d** The schematic semimetallic band portion around \bar{M} from **c**. The characteristic energy (E_0) is the charge neutral point of the semimetallic band portion corresponding to a pseudogap.

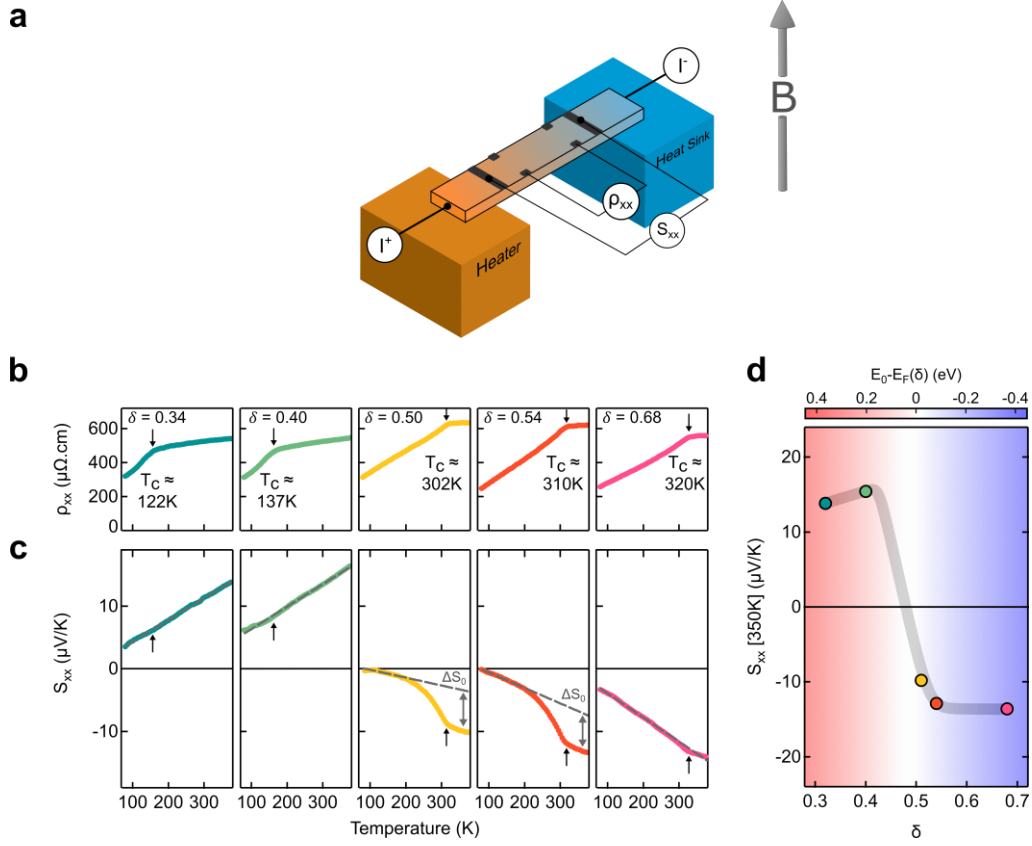


Fig. 2 Evolution of the transport properties in (001) oriented epitaxial $\text{Cr}_{1+\delta}\text{Te}_2$ films grown on Al_2O_3 (0001) substrates. **a** Electrode configuration for simultaneous measurement of longitudinal resistivity (ρ_{xx}) and thermopower (S_{xx}). The B -field is applied parallel to $\text{Cr}_{1+\delta}\text{Te}_2(001)$ direction. **b** Temperature and doping evolution of ρ_{xx} . T_c is estimated from the kinks in $\rho_{xx}(T)$. **c** Temperature dependence of S_{xx} . Arrows denote T_c from **b**. While $\delta < 0.5$ samples exhibit positive S_{xx} values with a nearly linear T-dependence, $\delta > 0.5$ samples exhibit negative S_{xx} values and anomalous curvature around T_c . **d** Doping evolution of S_{xx} at 350K with $E_0 - E_F(\delta)$ from 35 overlaid as a gradient showing a clear sign crossover in both quantities around $\delta = 0.5$.

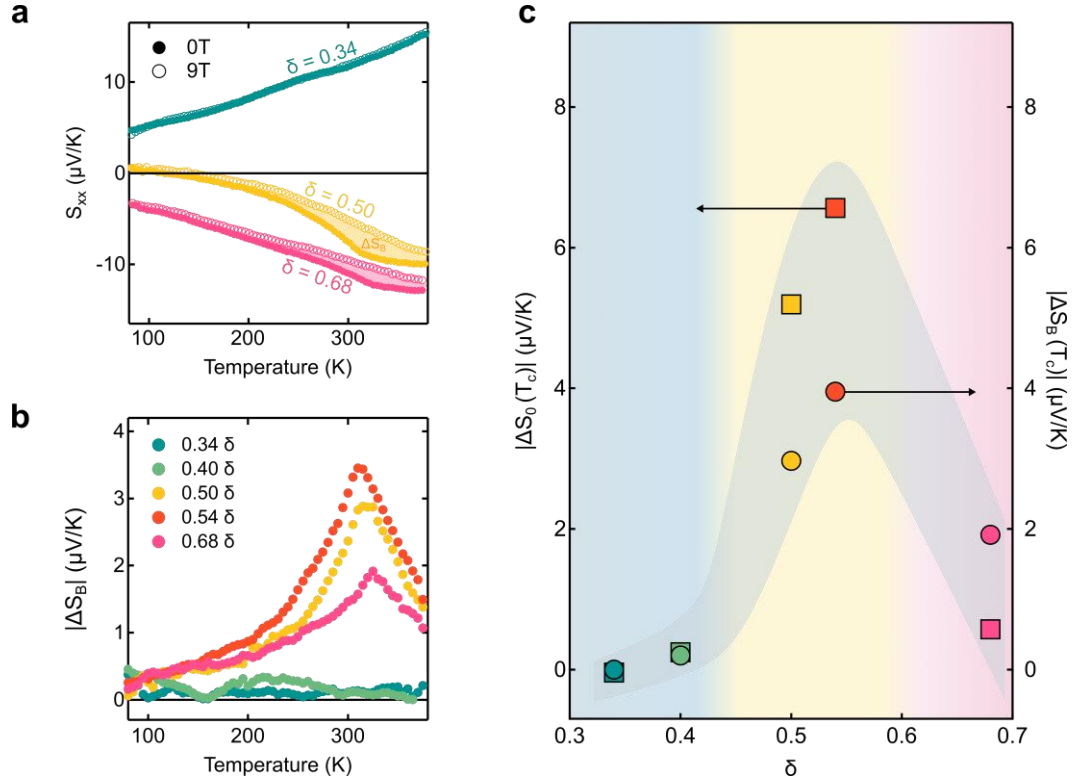


Fig. 3 Doping-dependent evolution of the magnetism-related thermopower in $\text{Cr}_{1+\delta}\text{Te}_2$. **a** $S_{xx}(T)$ for $\delta = 0.3$, 0.5 and 0.7 in 0T and 9T . **b** $|\Delta S_B| = |S(9\text{T}) - S(0\text{T})|$ shows the doping evolution of the field-dependent thermopower for the $\delta = 0.3, 0.5$ and 0.7 samples from **a**. As with $|\Delta S_0|$, $|\Delta S_B|$ also shows a maximum around $\delta_c \sim 0.5$, suggesting that magnetic frustration is the origin of the T_c anomaly in $\delta \sim 0.5$. **c** The phenomenological correspondence in the doping evolution of $|\Delta S_0|$ and $|\Delta S_B|$, with both quantities exhibiting maximums around $\delta_c \sim 0.5$, the composition that hosts maximum magnetic frustration, as indicated in **Fig. 1 b**. Shadows are meant merely as a guide to the eye.

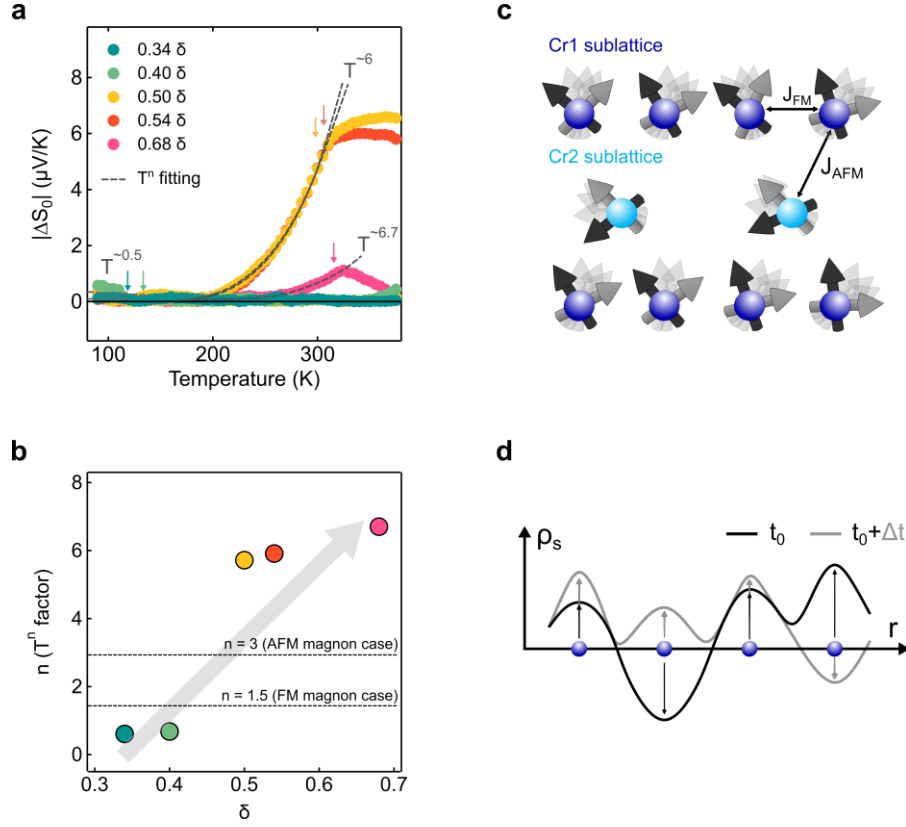


Fig. 4 Magnetic and electronic origins of the $\delta \sim 0.5$ anomalies in $\text{Cr}_{1+\delta}\text{Te}_2$. **a** The temperature dependence of the linear thermopower component $|\Delta S_0(T)| = |S_{xx}(T) - S_{\text{linear}}(T)|$ measures the degree of deviation from the T-linear behavior and shows a maximum around $\delta_c \sim 0.5$. Colored arrows indicate the position of T_c for the respective doping levels. Grey dotted lines indicate T^n fittings of the rising edge to T_c for each doping level. **b** The doping dependence of the critical exponent n from the T^n fittings in **a**. Values of n in the $\delta = 0.5$, $\delta = 0.54$, and $\delta = 0.68$ all exhibit exponents greater than the maximums expected from magnonic thermopower in the FM ($n = 1.5$) or AFM ($n = 3$) cases, which favors a spin fluctuation interpretation of thermopower enhancement. The shaded arrow is meant as a guide to the eye. **c** The schematic for spin fluctuation in S_{xx} at $\delta_c \sim 0.5$ (see the main body for details). **d** A schematic for how spin fluctuation density can vary in both space and time, contributing to charge entropy and consequently enhancing the thermopower in $\text{Cr}_{1+\delta}\text{Te}_2$.

References

- ¹ L. E. Bell, *Science* **321**, 1457–1461 (2008)
- ² W. Koshibae, K. Tsutsui, and S. Maekawa, *Phys Rev B*, **62**, 6869–6872, (2000)
- ³ I. Terasaki, Y. Sasago, and K. Uchinokura, *Phys Rev B*, **56**, R12685–R12687, (1997)
- ⁴ Y. Wang, N. S. Rogado, R. J. Cava, and N. P. Ong, *Nature*, **423**, 425–428 (2003)
- ⁵ T. Takeuchi et al., *Phys Rev B*, **69**, 125410 (2004)
- ⁶ G. E. W. Bauer, E. Saitoh, and B. J. van Wees, *Nat Mater*, **11**, 391–399 (2012)
- ⁷ K. Uchida et al., *Nature*, **455**, 778–781 (2008)
- ⁸ K. Uchida et al., *Nat Mater*, **9**, 894–897 (2010)
- ⁹ M. V. Costache, G. Bridoux, I. Neumann, and S. O. Valenzuela, *Nat Mater*, **11**, 199–202 (2012)
- ¹⁰ Md. M. H. Polash, F. Mohaddes, M. Rasoulianboroujeni, and D. Vashae, *J Mater Chem C*, **8**, 4049–4057 (2020).
- ¹¹ S. Nakatsuji and R. Arita, *Annu. Rev. Condens. Matter Phys.* 2022. 13:119–42
- ¹² C. Fu, Y. Sun, and C. Felser, *Appl. Mater*, **8**, 040913, (2020).
- ¹³ Y. Fujishiro et al., *Nat Commun*, **9**, 408 (2018).
- ¹⁴ C. Han, Q. Sun, Z. Li, and S. X. Dou, *Adv Energy Mater*, **6**, 1600498 (2016).
- ¹⁵ J. Yan, X. Luo, G. Lin, et al., *EPL* **124**, 67005 (2018).
- ¹⁶ Y. Wang, J. Yan, J. Li, et al., *Phys. Rev. B* **100**, 024434 (2019).
- ¹⁷ Z. Z. Jiang et al., *Phys. Rev. B* **102**, 144433 (2020).
- ¹⁸ Hashimoto, T., Hoya, K., Yamaguchi, M. & Ichitsubo, I., *J. Phys. Soc. Jpn.* 31, 679-682 (1971).
- ¹⁹ Dijkstra, J., Weitering, H.H., Bruggen, C.F.V., Haas, C. & Groot, R.A.D. *J. Phys. Condens. Matter* **1**, 9141 (1989).
- ²⁰ Yamaguchi, M. & Hashimoto, T. *J. Phys. Soc. Jpn.* **32**, 635-638 (1972).
- ²¹ Oda, K., Yoshii, S., Yasui, Y. et al. *J. Phys. Soc. Jpn.* **10**, 2999-3005 (2001).
- ²² L. Z. Zhang, A. L. Zhang, X. D. He et al. *Phys. Rev. B* **101**, 214413 (2020).

-
- ²³ G. Cao, Q. Zhang, M. Frontzek, et al. *Phys. Rev. Materials* **3**, 125001 (2019).
- ²⁴ Ohsawa, A., Yamaguchi, Y., Kazama, N., Yamaguchi, H. & Watanabe, H., *J. Phys. Soc. Jpn.* **33**, 1303-1307 (1972).
- ²⁵ Zhang, X., Lu, Q., Liu, W. et al., *Nat Commun* **12**, 2492 (2021).
- ²⁶ Huang, M., Gao, L., Zhang, Y., et al., *Nano Letter* **21**, 4280 (2021).
- ²⁷ He, Y., Kroder, J., Gayles, J. et al., *Appl. Phys. Lett.* **117**, 052409 (2020).
- ²⁸ Zhang, L-Z., He, X-D., Zhang, A-L. et al., *APL Mater.* **8**, 031101 (2020).
- ²⁹ Xian, JJ., Wang, C., Nie, JH. et al., *Nat Commun* **13**, 257 (2022).
- ³⁰ Y. Gong, J. Sun, W. Hu, S. Li, W. Xu, G. Tan, and X. Tang, *Appl. Phys. Lett.* **120**, 023905 (2022)
- ³¹ M. Huang, S. Wang, Z. Wang, P. Liu, J. Xiang, C. Feng, X. Wang, Z. Zhang, Z. Wen, H. Xu, G. Yu, Y. Lu, W. Zhao, S. A. Yang, D. Hou, and B. Xiang, *ACS Nano* **15**, 9759 (2021)
- ³² Z. Jin, Z. Ji, Y. Zhong, Y. Jin, X. Hu, X. Zhang, L. Zhu, X. Huang, T. Li, X. Cai, and L. Zhou, *ACS Nano* **16**, 7572 (2022)
- ³³ R. Chua, J. Zhou, X. Yu, W. Yu, J. Gou, R. Zhu, L. Zhang, M. Liu, M. B. H. Breese, W. Chen, K. P. Loh, Y. P. Feng, M. Yang, Y. L. Huang, and A. T. S. Wee, *Adv. Mater.* **33**, 2103360 (2021)
- ³⁴ Y. Fujisawa et al., *Phys Rev Mater*, **4**, 114001 (2020).
- ³⁵ Y. Fujisawa et al., arXiv:2204.02518
- ³⁶ N. P. Ong., *Phys. Rev. B*, **43**, 193 (1991).
- ³⁷ Hébert, Sylvie, et al. *Science and Technology of Advanced Materials* vol. 22, no. 1, 2021.
- ³⁸ Cullity, B.D. and Graham, C.D., John Wiley & Sons, 2011.
- ³⁹ Y. Zheng et al., *Sci Adv*, **5**, eaat9461 (2019).
- ⁴⁰ S. J. Watzman et al., *Phys Rev B*, vol. 94, no. 14, p. 144407, 2016.
- ⁴¹ T. Moriya, *Spin Fluctuations in Itinerant Electron Magnetism*, Springer Science & Business Media, 1985.
- ⁴² Heremans, J. P., Thermal spin transport and spin in thermoelectrics. In *Advances in Thermoelectricity: Foundational Issues, Materials and Nanotechnology*, 2021.
- ⁴³ Z. Jiang et al., *Phys Rev B*, **102**, 144433 (2020).
- ⁴⁴ R. Mondal, R. Kulkarni, A. Thamizhavel, and A. Thamizhavel, *J Magn Magn Mater*, **483**, 27, (2019).

⁴⁵ M. H. Polash and D. Vashae, *Iscience*, **24**, 103356 (2021).

⁴⁶ Q. Q. Li, S. Li, D. Wu, Z. K. Ding, X. H. Cao, L. Huang, H. Pan, B. Li, K. Q. Chen, and X. D. Duan , *Appl. Phys. Lett.*, **119**, 162402 (2021).